

**Electric-field-induced superconductivity in electrochemically-etched
ultrathin FeSe films on SrTiO₃ and MgO**

J. Shiogai^{1,#}, Y. Ito¹, T. Mitsuhashi¹, T. Nojima¹, and A. Tsukazaki^{1,2}

¹*Institute for Materials Research, Tohoku University, Sendai 980-8577, Japan.*

²*PRESTO, Japan Science and Technology Agency (JST), Chiyoda-ku, Tokyo 102-0075,
Japan.*

#Correspondence to: junichi.shiogai@imr.tohoku.ac.jp

Among the recently discovered iron-based superconductors¹⁻³, ultrathin films of FeSe grown on SrTiO₃ substrates have uniquely evolved into a high superconducting-transition-temperature (T_C) material⁴⁻¹⁵. The mechanisms for the high- T_C superconductivity are ongoing debate mainly with the superconducting gap characterized with *in-situ* analysis for FeSe films grown by bottom-up molecular-beam epitaxy. Here, we demonstrate the alternative access to investigate the high- T_C superconductivity in ultrathin FeSe with top-down electrochemical etching technique in three-terminal transistor configuration. In addition to the high- T_C FeSe on SrTiO₃, the electrochemically etched ultrathin FeSe transistor on MgO also exhibits superconductivity around 40 K, implying that the application of electric-field effectively contributes to the high- T_C superconductivity in ultrathin FeSe regardless of substrate material. Moreover, the observable critical thickness for the high- T_C superconductivity is expanded up to 10-unit-cells under applying electric-field and the insulator-superconductor transition is electrostatically controlled. The present demonstration implies that the electric-field effect on both conduction and valence bands plays a crucial role for inducing high- T_C superconductivity in FeSe.

Iron selenide (FeSe) is one of the iron-based superconductors ($T_C \sim 8$ K)¹⁻³, which has tetragonal PbO structure consisting of the layered atomic stacking of iron and selenium along c -axis. In the single or two unit-cell FeSe films grown by the state-of-the-art bottom-up molecular beam epitaxy (MBE)⁴⁻¹⁵ on insulating SrTiO₃ (refs. 12-14) or Nb-doped SrTiO₃ (refs. 4-12 and 15), a large superconducting gap of about 20 meV has been proved by angle-resolved photoemission spectroscopy (ARPES)⁴⁻¹⁰ and scanning tunneling microscopy (STM)¹¹. Compared to the expected T_C as high as 65 K (ref. 6) or 80 K (ref. 11) from the large gap energy evaluated by ARPES or STM, temperature dependence of resistivity gauges the consensus of the onset T_C value about 40 K (refs. 11-14). However, a very recent report of superconductivity above 100 K detected by *in-situ* electrical resistance measurements for FeSe films grown on Nb-doped SrTiO₃ would make T_C become widespread^{15,16}. The mechanisms for the enhancement of superconducting gap energy in ultrathin FeSe are now discussed about strong electron-phonon coupling¹⁰, variation of the electronic band structure at M point and Γ point⁴, and charge transfer effect from substrates^{5,13}. *Ex-situ* characterizations based on temperature dependence of resistivity regarding electric-field effect, magnetic-field effect, thickness dependence of T_C and substrate material dependence are matters of interest for deep understanding the high- T_C superconductivity in ultrathin FeSe studies.

In contrast to the *in-situ* bottom-up MBE technique, a classical electrochemical etching¹⁷ is one of the best ways for top-down approach to the ultrathin FeSe films, because the uniform and fine tuning in thickness is possible with continuously monitoring electrical current originating from the electrochemical reaction. In our experiments, we employed this electrochemical etching approach in three-terminal transistor configuration, so-called an electric double layer (EDL) transistor (Fig. 1a)^{18,19}. The EDL transistors were fabricated from 13- and 18-nm-thick FeSe films grown on insulating SrTiO₃ and MgO substrates, respectively, by pulsed-laser deposition (PLD) as described in Methods. The films and Pt gate electrode are covered with an ionic liquid (IL) of DEME-TFSI as schematically shown in Fig. 1a. The original concept of the EDL transistor involves an electrostatic charge carrier doping based on giant capacitance originating from a very narrow (< 1 nm) EDL width. Following this concept, various kinds of physical properties such as superconductivity¹⁹, ferromagnetism^{20,21} and insulator-metal transition in correlated electron systems^{22,23} have been induced or controlled electrostatically. Another feature of EDL transistors is electrochemical reaction²⁴⁻²⁶. These two features of EDL transistor appear separately, depending on the temperature of IL and the applied gate voltage^{24,25}, with some boundary as schematically shown by the black broken line in Fig. 1b. In this study, we have applied

the electrostatic doping effect with V_G variation below the characteristic temperature (blue arrow in Fig. 1b) and the electrochemical etching to peel FeSe layers with tuning the sample temperature under V_G applied constant (red arrow in Fig. 1b). After each etching sequence, systematic thickness dependence and field-effect of the superconductivity in FeSe films can be investigated in a single EDL transistor.

Temperature dependence of the channel sheet resistance (R_s - T curve) and its superconducting properties were measured using a standard d. c. four-terminal method. In the initial thick films on SrTiO₃ and on MgO, the onset superconducting transition temperature $T_c^{\text{on}} = 8.2$ K and 4.8 K are clearly observed by lowering temperature T as shown in Fig. 1c (solid lines), which is consistent with the bulk properties of FeSe (ref. 3). No significant change in R_s - T curves (broken lines) is observed with electrostatic doping via $V_G = 5$ V at 220 K for the initial thick condition, implying that high- T_C superconductivity is not induced at IL/FeSe interface (see Supplementary Information) at this temperature.

The high- T_C superconductivity appears in both FeSe films grown on SrTiO₃ (sample A) and MgO (sample N) after a series of etching as shown in Fig. 2a and 2b, respectively. With carrying forward the etching sequence with applying $V_G = 5$ V at about 245 K and R_s - T measurements regularly under the constant V_G (black arrow in Fig.

1b), the onset T_C in normalized sheet resistance R_s/R_s^{100K} is drastically enhanced from the bulk value to the higher one of $T_c^{\text{on}} = 43.3$ and 39.0 K for sample A and N, respectively. The estimated T_c^{on} from R_s - T curves shown in Fig. 2a and 2b are summarized in Fig. 2c and 2d, respectively as a function of the averaged thickness, which is carefully estimated from the initial thickness and the etching rate in electrochemical reaction via the gate leakage current (see SI). Four implications are contained in these figures. The first is that the two-step transitions are observed in the intermediate etching region. Accompanying with the enhancement of metallic behavior, R_s drops first at around $T = 30$ K and second at 8 K and 4 K in the case of FeSe on SrTiO₃ and MgO, respectively, as a first signature of the appearance of high- T_C superconducting region in the device. The systematic disappearance of the bulky low- T_C region with decreasing thickness evidences our fine tuning of the thicknesses. Indeed, the zero resistance temperature of about 30 K implies that the FeSe layers are uniformly etched down to the one/two-unit-cells in our primitive devices. The second is that the high- T_C superconductivity emerges at the ultrathin FeSe film on MgO thanks to the electric-filed effect in EDL transistor. Such high- T_C superconductivity in FeSe on MgO has not been reported in *in-situ* MBE studies, which is probably due to no charge transfer from MgO to FeSe. The third is that the values of T_c^{on} for both samples on SrTiO₃ and MgO are

close to the highest values that have been reported in capped single-unit-cell FeSe films grown by MBE¹²⁻¹⁴. If the disorder at IL/FeSe interface limits T_c^{on} to about 40 K as low as the capped FeSe, we need further improvement of interface quality to enhance T_c^{on} toward 100 K (refs. 15 and 16). The forth is that the high- T_C superconductivity emerges under a relatively thicker condition about 10-unit-cells, followed by the small thickness dependence. At present, it is not clear whether whole thick film region contributes high- T_C superconductivity or not. We will discuss it later.

To further investigate the superconducting properties of the ultrathin FeSe film, we performed R_s - T measurements under perpendicular magnetic fields B for sample N on MgO. As shown in Fig. 2e, the tail of resistive transition is broadened by applying B indicating the two dimensional nature of the FeSe film. Figure 2f shows the temperature dependence of perpendicular upper critical field $B_{c2}(T)$ derived from the midpoint temperature of the resistance drop $T_c(B)$ in R_s - T curves in Fig. 2e. From the linear relation, which is consistent with the Ginzburg-Landau (GL) theory given as $B_{c2}(T) = \frac{\phi_0}{2\pi\xi^2(0)}(1 - T/T_c(0))$ with ϕ_0 and $\xi(0)$ being the flux quantum and the GL coherent length at zero temperature, respectively, we obtained $\xi(0) = 2.0$ nm, which is around two times shorter than the bulk value³.

Getting back to the thickness dependence of T_c^{on} in Figs. 2c and 2d, we note that the first single step superconducting transition appears at the thickness of 9.6 nm and 5.9 nm for sample A and N, respectively. The appearance of high- T_C superconductivity in the rather thicker conditions offers us to consider that how the electric-field effect contributes to the high- T_C superconductivity. Here, we examined the effect of electrostatic doping on the superconductivity in both ultrathin and thicker conditions by different experimental schemes in the same device set-up as sample A. At first, samples B, C on SrTiO₃ and M on MgO were etched at $T = 245$ K to induce the superconductivity as shown in Fig. 3a, the top panel of Fig. 3c and Fig. 3d (red line data), respectively. The thicknesses of samples B, C and M are tuned to the one/two-unit-cell (the red square in Fig. 2c), 9.4 nm (the blue triangle in Fig. 2c) and 3.7 nm (the green circle in Fig. 2d), respectively, by monitoring the leakage current under the assumption that the same etching rate with sample A holds. After the detection of the high- T_C superconducting behavior, we examined the electrostatic effect with removing and then applying V_G at $T = 220$ K (along the blue arrow in Fig. 1b; Note that no electrochemical etching occurs at this temperature as mentioned above).

For sample B expectedly in the one/two-unit-cell condition, the initial insulating behavior was not recovered by removing V_G from 5 V to 3 and 0 V as shown in Fig. 3b.

This result is a good evidence for the thickness reached close to one/two-unit-cell, because the high- T_C superconductivity under $V_G = 0$ V is consistent with the result of previous reports on FeSe/SrTiO₃ with charge transfer solely from the SrTiO₃ substrate⁸. Interestingly, the increase of T_c^{on} from 43.5 K to 46.3 K as a result of reduced V_G implicates the over-doping effect by electrostatic doping. In contrast, in sample C under the thicker 9.4 nm condition, the superconductivity vanishes and the R_s - T curve is back to the insulating behavior when V_G is removed (blue line in middle panel of Fig. 3c). The reappearance of insulating behavior indicates the uniform etching without local ultrathin region providing a high- T_C superconducting current pass. Then, application of $V_G = 5$ V recovers the superconductivity again (blue line in bottom panel of Fig. 3c), demonstrating a reversible control of insulator-superconductor transition by electrostatic mean. These series of results in sample C suggests that the observable thickness condition for high- T_c^{on} superconductivity is widely expanded from one/two-unit-cell to above 10-unit-cells by the application of electric field. Additionally, T_c^{on} in sample M decreases with reducing the accumulated charge as shown in Fig. 3d. Therefore, we suppose that the high- T_C superconductivity in ultrathin FeSe on MgO is fully controllable by the application of electric-field effect.

Finally, we discuss possible mechanisms for the high- T_C superconductivity in FeSe EDL transistor from the view point of the thickness dependence. The comparable values of T_c^{on} as shown in Fig. 2c and 2d for SrTiO₃ and MgO suggests that the electric-field effect induces superconductivity at 40 K despite that one may expect the different electron-phonon coupling between FeSe film and substrate¹⁰. Concomitantly, the small thickness dependence of T_c^{on} below 10-unit-cell indicates that an ultrathin condition, particularly single-unit-cell itself, does not probably play a crucial role to the increase of T_C in ultrathin FeSe superconductivity. Nevertheless, the origin for the difference of critical thickness for SrTiO₃ (9.6 nm) and MgO (5.9 nm) is still not clear at present although it may link to the degree of charge transfer from substrates to FeSe. Naively, it is likely that the positive V_G depletes holes in the valence band at the Γ point and accumulates electrons in the conduction band at the M point through the IL/FeSe interface, while the interface between IL and thick FeSe layer does not work as the high- T_C superconducting channel (see Fig. 1c). As a consequence, the similar modification of the electronic band structure at the Γ and M point, as is proved by ARPES for the single-unit-cell FeSe on SrTiO₃ exhibiting large superconducting gap energy⁵, may be realized by applying electric-field below the critical thicknesses on

SrTiO₃ and MgO. However, we need further investigation about the modification of electronic band structures under V_G application to verify our speculation.

By employing EDL transistor configuration, the high- T_C superconductivity in ultrathin FeSe films has been investigated from the several aspects such as thickness and substrate material dependence. The application of electric-field effect inducing modification of electronic band structure would make a major contribution for T_c^{on} of 40 K below 10-unit-cells regardless of substrate material. Our demonstration of the etching well controlled by the temperature of IL under applying V_G shed light to the new aspect of the EDL transistor that is a useful approach to ultrathin films studies, expanding an opportunities to exemplify *ex-situ* the superconductivity of ultrathin FeSe grown on various insulating substrates^{12,13,15,27}.

Methods

Sample fabrication. The FeSe films were grown at 300 °C on insulating SrTiO₃ (001) and MgO (001) substrates by pulsed-laser deposition with as-delivered FeSe target (Kojundo Chemical Laboratory Co., Ltd), which was followed by the *in-situ* post annealing at 450 °C for 30 min. The growth rate with laser repetition rate of 5 Hz is

approximately 17 nm/h, whose value is estimated by x-ray Laue fringes (See SI). After cutting the film into a $2 \times 5 \text{ mm}^2$ rectangular piece, the channel and the four-terminal electrode (indium pads) were prepared to confine the current flow within the channel by scratching the film. Then, the electrodes were covered by silicone sealant to prevent them from chemical reaction with the ionic liquid. A platinum plate for the side gate electrode was placed next to the FeSe channel on the same chip and indium pads are attached on the gate electrode in the same way (See SI). Then, the FeSe channel and the gate electrode are covered by the ionic liquid, *N,N*-dethyl-*N*-methyl-*N*-(2-methoxyethyl)ammonium bis(trifluoromethanesulfonyl)imide (DEME-TFSI) to form electric double layer transistor configuration as shown in Fig. 1a. To suppress the degradation of the sample in the air, we carried out the EDL fabrication process as soon as possible. However, it usually took 6 hours before starting the measurement and the sample surface was inevitably exposed to the air about 2-3 hours.

Electrical measurements. The sheet resistance R_s is measured by standard four-terminal method where a constant current of typically $0.5 \text{ }\mu\text{A}$ is applied and the longitudinal voltage drop is measured by a nano-voltmeter. Temperature is controlled by dipping the sample into the liquid helium vessel in electrical measurements for samples A - C.

Sample temperature is monitored by a calibrated resistance thermometer (Cernox1050 resistor) inserted in the copper block where the sample is mounted. The R_s - T curve and magnetotransport properties for samples M and N are measured by Quantum Design Physical Property Measurement System (PPMS). To control the doping level electrostatically through EDL tuning, we fix the temperature at $T = 220$ K during V_G variation. In contrast, the occurrence of the electrochemical reaction has been checked by tuning T within the range from 240 K to 250 K with keeping the $V_G = 5.0$ V constant.

Acknowledgments

The authors thank S. Tanaka and T. Ouchi for experimental help and M. Kawasaki, Y. Iwasa and K. Fujiwara for stimulating discussions. This work is partly supported by Grant-in-Aid for Scientific Research on Innovative Areas (No. KAKENHI 22103004) from MEXT of Japan and Grant-in-Aid for Specially Promoted Research (No. KAKENHI 25000003) from the Japan Society for the Promotion of Science (JSPS).

Author contributions

J. S., T. N. and A. T. conceived and designed this research. Y. I. and J. S. performed thin films growth and electrical measurements. T. M. and T. N. prepared electrical measurement system for EDL transistor device configuration in liquid helium vessel. Y. I. and J. S. analyzed the data and all authors jointly discussed. J. S. and A. T. wrote the manuscript and all authors commented on the manuscript.

Competing financial interests

The authors declare no competing financial interests.

References

1. Kamihara, Y., Watanabe, T., Hirano, M. & Hosono, H., Iron-based layered superconductor $\text{La}[\text{O}_{1-x}\text{F}_x]\text{FeAs}$ ($x = 0.05\text{--}0.12$) with $T_c = 26$ K. *J. Am. Chem. Soc.* **130**, 3296-3297 (2008).
2. Haindl, S. *et al.*, Thin film growth of Fe-based superconductors: from fundamental properties to functional devices. A comparative review. *Rep. Prog. Phys.* **77**, 046502 (2014).

3. Hsu, F. C. *et al.*, Superconductivity in the PbO-type structure α -FeSe. *Proc. Natl. Acad. Sci. USA* **105**, 14262-14264 (2008).
4. Liu, D. *et al.*, Electronic origin of high-temperature superconductivity in single-layer FeSe superconductor. *Nature Commun.* **3**, 931 (2012). doi: 10.1038/ncomms1946.
5. He, S. *et al.*, Phase diagram and electronic indication of high-temperature superconductivity at 65 K in single-layer FeSe films. *Nature Mater.* **12**, 605-610 (2013).
6. Tan, S. *et al.*, Interface-induced superconductivity and strain-dependent spin density waves in FeSe/SrTiO₃ thin films. *Nature Mater.* **12**, 634-640 (2013).
7. Peng, R. *et al.*, Measurement of an enhanced superconducting phase and a pronounced anisotropy of the energy gap of a strained FeSe single layer in FeSe/Nb:SrTiO₃/KTaO₃ heterostructures using photoemission spectroscopy. *Phys. Rev. Lett.* **112**, 107001 (2014).
8. Peng, R. *et al.*, Tuning the band structure and superconductivity in single-layer FeSe by interface engineering. *Nature Commun.* **5**, 5044 (2014). doi: 10.1038/ncomms6044.

9. Liu, X. *et al.*, Dichotomy of the electronic structure and superconductivity between single-layer and double-layer FeSe/SrTiO₃ films. *Nature Commun.* **5**, 5047 (2014).
Doi: 10.1038/ncomms6047.
10. Lee, J. J. *et al.*, Interfacial mode coupling as the origin of the enhancement of T_c in FeSe films on SrTiO₃. *Nature* **515**, 245-248 (2014).
11. Wang, Q. Y. *et al.*, Interface-induced high-temperature superconductivity in single unit-cell FeSe films on SrTiO₃. *Chin. Phys. Lett.* **29**, 037402 (2012).
12. Sun, Y. *et al.*, High temperature superconducting FeSe films on SrTiO₃ substrates. *Sci. Rep.* **4**, 6040 (2014). doi: 10.1038/srep06040.
13. Zhang, W. *et al.*, Interface charge doping effects on superconductivity of single-unit-cell FeSe films on SrTiO₃ substrates, *Phys. Rev. B* **89**, 060506(R) (2014).
14. Zhang, W. H. *et al.*, Direct observation of high-temperature superconductivity in one-unit-cell FeSe films. *Chin. Phys. Lett.* **31**, 017401 (2014).
15. Ge, J. F. *et al.*, Superconductivity above 100 K in single-layer FeSe films on doped SrTiO₃. *Nature Mater.* **14**, 285-289 (2015).

16. Bozovic, I. & Ahn, C., A new frontier for superconductivity. *Nature Phys.* **10**, 892-895 (2014).
17. Simon, P. & Gogotsi, Y., Materials for electrochemical capacitors. *Nature Mater.* **7**, 845-854 (2008).
18. Shimotani, H., Diguët, G. & Iwasa, Y., Direct comparison of field-effect and electrochemical doping in regioregular poly(3-hexylthiophene). *Appl. Phys. Lett.* **86**, 022104 (2005).
19. Ueno, K. *et al.*, Field-induced superconductivity in electric double layer transistors. *J. Phys. Soc. Jpn.* **83**, 032001 (2014) and references therein.
20. Yamada, Y. *et al.*, Electrically induced ferromagnetism at room temperature in Cobalt-doped titanium dioxide. *Science* **332**, 1065-1067 (2011).
21. Shimamura, K. *et al.*, Electrical control of Curie temperature in cobalt using an ionic liquid film. *Appl. Phys. Lett.* **100**, 122402 (2012).
22. Nakano, M. *et al.*, Collective bulk carrier delocalization driven by electrostatic surface charge accumulation. *Nature* **487**, 459-462 (2012).
23. Jeong, J. *et al.*, Suppression of metal-insulator transition in VO₂ by electric field-induced oxygen vacancy formation. *Science* **339**, 1402-1405 (2013).

24. Yuan, H. *et al.*, Electrostatic and electrochemical nature of liquid-gated electric-double-layer transistors based on oxide semiconductors. *J. Am. Chem. Soc.* **132**, 18402-18407 (2010).
25. Ueno, K., Shimotani, H., Iwasa, Y. & Kawasaki, M., Electrostatic charge accumulation versus electrochemical doping in SrTiO₃ electric double layer transistors. *Appl. Phys. Lett.* **96**, 252107 (2010).
26. Nojima, T. *et al.*, Hole reduction and electron accumulation in YBa₂Cu₃O_y thin films using an electrochemical technique: Evidence for an *n*-type metallic state. *Phys. Rev. B* **84**, 020502(R) (2011).
27. Bang, J. *et al.*, Atomic and electronic structures of single-layer FeSe on SrTiO₃ (001): The role of oxygen deficiency. *Phys. Rev. B* **87**, 220503(R) (2013).

Figure captions

Figure 1| Electrochemical etching and electrostatic doping in electric double layer transistor. **a**, Schematic of the EDL transistor composed of FeSe films on insulating SrTiO₃ and MgO substrates. Side gate voltage V_G is applied through the ionic liquid. The gate leakage current I_G is measured by picoammeter, which is a measure for the degree of etching. **b**, Schematic diagram displaying the role of EDL transistor as a function of V_G and temperature T . The broken line indicates a kind of boundary between electrostatic doping and electrochemical etching. **c**, The R_s - T curves of sample A on SrTiO₃ and sample M on MgO for initial thick condition when $V_G = 0$ V (solid lines) and 5 V (broken lines) are applied.

Figure 2| Thickness tuning of FeSe on SrTiO₃ and MgO via electrochemical etching. **a,b**, Sheet resistance normalized to the value at $T = 100$ K, R_s/R_s^{100K} , as a function of temperature T for continuing etching processes *i.e.*, different film thickness (d), for sample A on SrTiO₃ and for sample N on MgO, respectively. The onset superconducting transition temperature T_c^{on} is defined by the intersection of the broken two linear extrapolation lines. **c,d**, T_c^{on} for samples A and N shown in Fig. 2a and 2b, respectively, are collected as a function of averaged thickness for the electric-field

induced high- T_C (E -induced; filled black circles) and the initial bulk-like low- T_C (open black circles) conditions. A vertical broken line corresponds to the thickness for the first data showing single step transition in R_s - T curves. The data for samples B, C and M after etching and at $V_G = 5$ V are indicated by red square, blue triangle and green circle, respectively. **e**, Perpendicular magnetic field dependence of R_s - T curves of sample N after etching down to $d = 0.5$ nm measured at $B = 0, 1, 3, 5, 7$ and 9 T. **f**, Temperature dependence of the upper critical field $B_{c2}(T)$ derived from the midpoint of the resistance drop in Fig. 2e. Red line corresponds a linear fitting line based on the GL theory.

Figure 3 | Electrostatic tuning of superconductivity. **a**, Normalized sheet resistance R_s/R_s^{100K} as a function of temperature T for sample B in the initial 13-nm-thick state with applied $V_G = 5$ V (gray solid line) and after etching down to one unit-cell with $V_G = 5$ V (red solid line). **b**, The R_s - T data for sample B after thinning to the 0.5 nm. V_G is reduced from $V_G = 5$ V (red), 3 V (green), to 0 V (gray). **c**, The reversible variation in T dependence of R_s/R_s^{100K} for sample C against V_G . (Top panel) The initial insulating (13 nm thick) states with $V_G = 5$ V (gray solid line) and the superconducting behavior after the electrochemical etching to 9.4-nm-thick condition at $V_G = 5$ V (blue). (Middle panel) Blue solid line shows R_s/R_s^{100K} after removing V_G to 0 V. (Bottom panel) Blue solid line

shows R_s/R_s^{100K} with the second application of $V_G = 5$ V. **d**, The R_s - T curves measured for sample M under 3.7 nm condition. Transition behavior is presented as reducing charges from red solid line (charged at $V_G = 5$ V) to blue solid line (discharged at $V_G = 0$). Triangles correspond to the T_c^{on} .

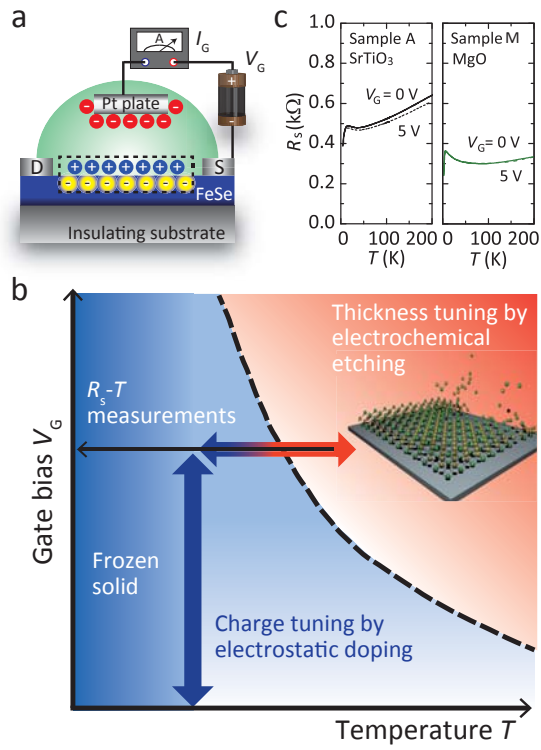


Figure 1 J. Shioyai *et al.*,

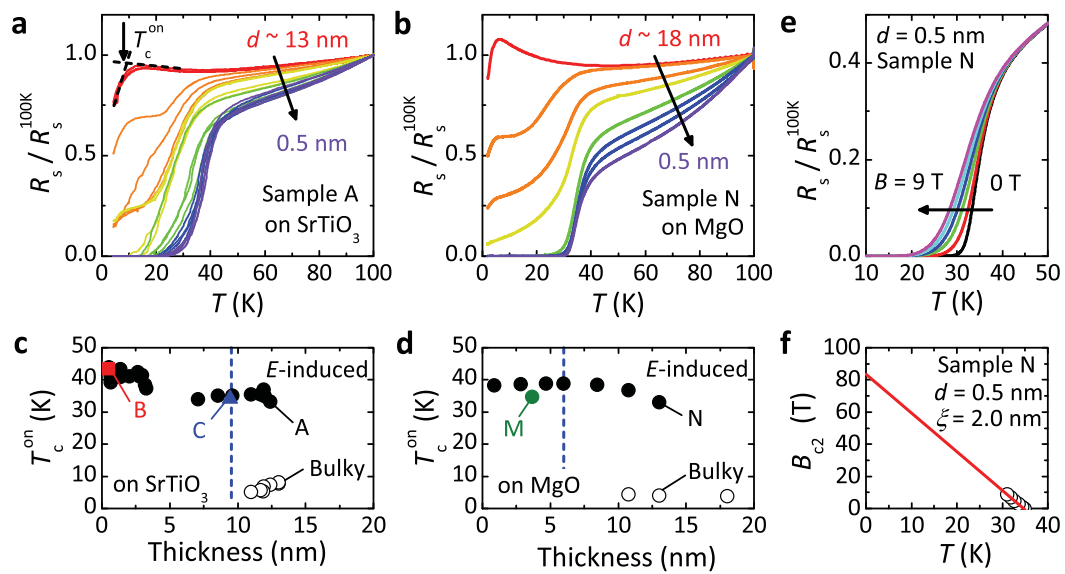


Figure 2 J. Shiogai *et al.*,

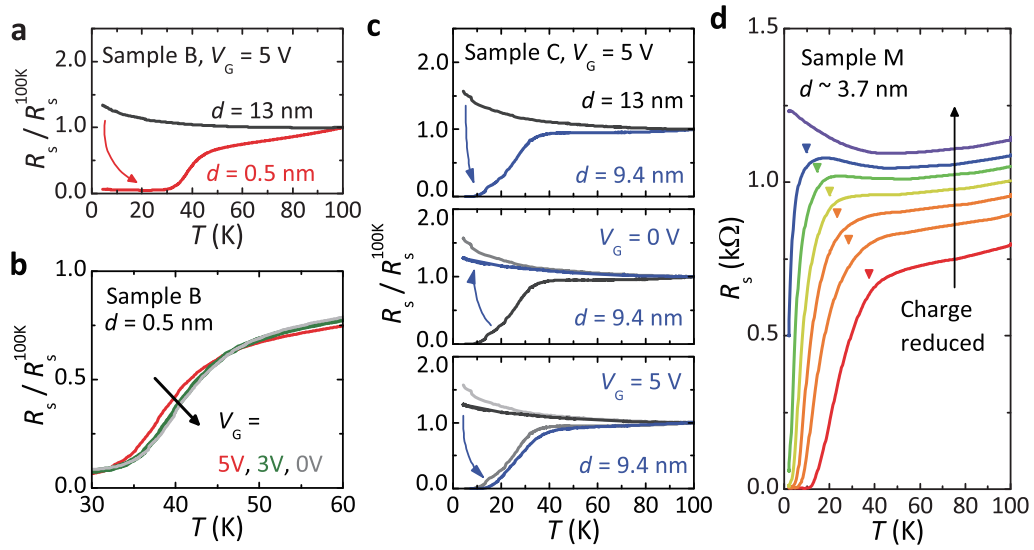


Figure 3 J. Shiogai *et al.*,